Single-Event Transients in SiGe HBTs Induced by Pulsed X-Ray Microbeam

Delgermaa Nergui, *Student Member, IEEE*, Adrian Ildefonso, *Student Member, IEEE,* George N. Tzintzarov, *Student Member, IEEE*, Nelson E. Lourenco, *Member, IEEE,* Anup P. Omprakash, *Member, IEEE*, Patrick S. Goley, *Student Member, IEEE,* Zachary E. Fleetwood, *Member, IEEE*, Stephen D. LaLumondiere, *Member, IEEE,* Jeremy P. Bonsall, Daniele M. Monahan, Hunter Kettering, Dale L. Brewe, and John D. Cressler, *Fellow, IEEE*

***Abstract*—The first experimental study of single-event transients induced by pulsed X-rays in SiGe HBTs. Device-level transient data and circuit-level upset data from pulsed X-rays are analyzed and compared to those of heavy ions. 2-D TCAD modeling is utilized to understand the source of the differences in the transients. The transient peak from ion-shunt effect is not present in pulsed X-ray transients due to its large spot size and slow pulse transition, both of which lead to lower peak carrier densities. The diffusion "tail", typically present in transients measured from SiGe HBTs, also differs between the two sources. The charge collection of X-ray has a linear correlation with surface LET across the photon energies of 8-12 keV. For a similar surface LET, the impinging heavy ion pushes the transient subcollector-substrate junction boundaries of the SiGe HBT deeper, resulting in higher charge collection. SEU screening of shift-registers show that X-ray can detect device sensitive nodes smaller than the beam.**

***Index Terms*—pulsed X-ray testing, radiation effects, single-event effects (SEE), SiGe HBTs, charge collection, TCAD**

I. Introduction

SILICON-GERMANIUM (SiGe) technologies integrate high-speed SiGe heterojunction bipolar transistors (HBTs) with conventional silicon CMOS. SiGe HBTs offer inherent high tolerance to total ionizing dose and displacement damage, making it suitable for space-based applications. However, SiGe HBTs are highly susceptible to single-event effects (SEEs), with data upset cross-sections that can exceed the active area of the device. This vulnerability has prompted extensive recent investigations on radiation-induced transient characteristics, a summary of which can be found in [1].

Two commonly utilized sources for SEE investigations are heavy ion beams and pulsed lasers. Most heavy-ion testing is performed using a broadbeam, with no information about the strike location, while focused ion beam facilities often have limited penetration depth due to energy constraints or are of limited availability. Pulsed lasers, on the other hand, are more cost-effective and give valuable spatial information for circuit screening [2]. However, such lasers cannot penetrate metals that typically cover the sensitive regions of devices and circuits. Carrier generation induced by two-photon absorption can be accomplished from the backside to avoid any beam interactions with the metal, but it can require additional processing such as backside surface polishing. Recent studies have shown that pulsed focused X-ray beams can also be used for SEE investigations [3]. X-rays have a deep penetration depth, which is essential for use in SiGe HBT single-event transient (SET) studies due to their very deep sensitive volume [4].

In the present work, X-ray-induced charge collection mechanisms in SiGe HBTs are investigated for the first time. The resulting SETs are compared to heavy-ion induced transients to identify the potential uses and limitations of pulsed X-rays in SEE testing of SiGe HBTs. TCAD simulations are employed to understand some of the observed differences between pulsed X-ray and ion data. The device-level study shows that, for circuits built using SiGe HBTs, pulsed X-rays are best suited for SEE testing when the main error metric (e.g., single-event upsets) is directly tied to the collected charge. Single-Event Upset (SEU) in a master-slave (MS) shift-register (SR) induced by X-ray and heavy ion are compared for potential utilization of X-ray in circuit screening. The X-ray beam was able to show the sensitives nodes of the circuit. However, circuit-level correlation of ion and X-ray LET proved to require more in-depth analysis and is beyond the scope of this paper.

II. Experimental Setup

A. Experimental Setup and Device Under Test

Pulsed X-ray experiments were performed at beamline 20-ID-B of the Advanced Photon Source (APS) at Argonne National Laboratory. X-ray energies between 4-27 keV are available at the beamline. The details about the beamline can be found in [5]. X-Ray beams with 8-12 keV photon energies, with a flux up to $5x10^{11}$ photons/s, 102 ps half width at $1/e^2$ intensity, and 1.61 – 1.7 µm focused beam radius at $1/e^2$ intensity were used in this investigation. The photon energies utilized, their

D. Nergui, A. Ildefonso, G. N. Tzintzarov, P. S. Goley and J. D. Cressler are with the School of Electrical and Computer Engineering, 777 Atlantic Drive, NW, Georgia Institute of Technology, Atlanta, GA 30332-0250 USA (email: dnergui3@gatech.edu, cressler@ece.gatech.edu).

N. E. Lourenco is with Georgia Tech Research Institute, Atlanta, GA 30332 USA.

A. P. Omprakash was with Georgia Institute of Technology, Atlanta, GA 30332 USA. He is now with Raytheon Company, El Segundo, CA 90245 USA.

Z. E. Fleetwood is with SpaceX, Redmond, WA 98052 USA.

S. D. LaLumondiere, J. P. Bonsall, D. M. Monahan, H. Kettering are with The Aerospace Corporation, Los Angeles, CA 90009 USA.

D. L. Brewe is with the Advanced Photon Source, Argonne, IL 60439 USA.

TABLE I
X-RAY BEAM PROPERTIES

Photon Energy (keV)	Absorption Coefficient (cm^{-1})	Penetration Depth (μm)
8.0	148.6	67
10.0	77.1	130
11.3	56.5	177
12.0	44.7	224

respective absorption coefficients, and 1/e penetration depths in silicon, are given in Table I [6].

The device was irradiated only when data were taken (i.e., the transient from every pulse was recorded to avoid excessive dose). The Gummel characteristics were measured periodically throughout the experiments and showed no change due to irradiation, which implies that the total dose received by the samples was not significant enough to cause electrical performance degradation.

The heavy-ion experiments were performed using the 10-MeV/amu cocktail at the 88-inch cyclotron BASE facility at the Lawrence Berkeley National Laboratory. The experimental results presented were obtained using the GlobalFoundries' third-generation technology, 8HP SiGe BiCMOS platform (200 GHz f_T / 285 GHz f_{max}). An NPN SiGe HBT with CBEBC layout and the emitter area of 0.12x10.00 μm^2 was used for the device study. A standard (unhardened) master-slave (MS) shift register (SR) with hardened clock trees was used for the SEU experiment. All of the transistors in the SR are CBE NPN SiGe HBTs with an emitter area of 0.12x1.00 μm^2. The devices-under-test (DUT) were wirebonded to custom-made, high-speed printed circuit boards. The transients were captured using a Tektronix 12.5 GHz DPO71254 real-time oscilloscope. The SEU error rates were measured using Anritsu MP1761B Pulse Pattern Generator and MP1762A Error Detector.

B. TCAD Simulation Setup

To further investigate the measurement results, calibrated 2-D TCAD simulations were performed using Synopsys Sentaurus. The device in the simulation bench has similar DC and AC characteristics as the SiGe HBTs used for the heavy-ion and X-ray experiments. The LET from SRIM was incorporated into TCAD to simulate transistor-level charge collection from heavy ion strikes. The charge deposition profile of X-ray beam was calculated and incorporated into the Sentaurus TCAD tool through their physical model interface, using (1). Charge collection due to pulsed X-ray was then simulated using these modified charge deposition profiles. The cross-section of the HBT model, along with an example of an X-ray charge deposition profile is shown in Fig. 1.

III. HEAVY-ION AND X-RAY CHARGE DEPOSITION

The intensity of the pulsed X-ray beam, assumed to be Gaussian, has a spatial and temporal shape expressed by Gaussian beam propagation. The intensity of the beam can be described in the radial (r) and axial (z) directions, as well as in the time (t) domain by [7],

$$I(r,z,t) = I_0 e^{-\left(\frac{2r^2}{w_0^2}\right)} e^{-\alpha z} e^{-\left(\frac{2t^2}{\tau^2}\right)} \quad (1)$$

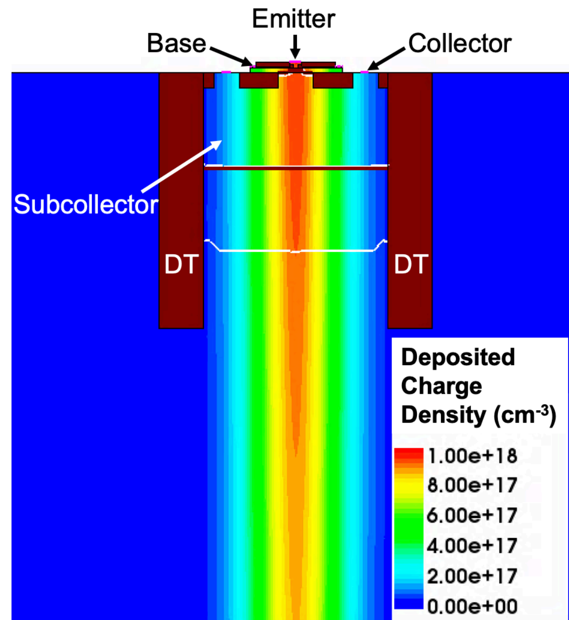

Fig. 1. TCAD cross-section of the IBM 8HP SiGe HBT. The cross-section shows the simulated charge density profile of a representative X-ray pulse with 296 pJ pulse energy and 10 keV photon energy is shown.

where w_0 is the beam radius at the 1/e^2 intensity, τ is the half width of the beam at the 1/e^2 intensity, and α is the material absorption coefficient. The beam is well collimated throughout the silicon depth since the X-ray wavelength is four orders of magnitude smaller than its spot size [5]. When the beam is incident on the device, it loses some of its energy in the device back-end-of-line (BEOL) metals and inter-metal dielectrics. The transmission factor, T, of the incident beam through n layers of metals and oxides can be defined as

$$T = \exp(\sum_{i=1}^{n} -\alpha_i t_i) \quad (2)$$

where α_i is the material absorption coefficient, and t_i is the thickness of the layer. Since the transmission factor depends on location, the best- and worst-case scenarios are calculated. The best-case occurs when the beam only penetrates oxide layers, while the worst-case is when the beam penetrates all the metal and oxide layers that are in the BEOL. These bounds give a range of X-ray pulse energies when it reaches the silicon surface. The thickness of each layer was obtained from the technology process design kit, and the absorption coefficients were obtained from the X-ray mass attenuation coefficient in [6]. The calculated transmission factors for those best- and worst-case scenarios for each photon energy are summarized in Table II. For some photon energies, such as 10 keV, the difference is quite high, nearly 50%. The transmission factor highly depends on the type of material and photon energy. Therefore, knowing the BEOL layers of the DUT is necessary for accurate dosimetry at the silicon surface. If the BEOL layers are not known, higher photon energy beam can be used to avoid high energy loss.

The LET of an ion, defined as the charge deposition per unit length in a given material, is the typical metric used in heavy-

TABLE II
X-RAY TRANSMISSION THROUGH DEVICE BEOL

Photon Energy (keV)	Transmission Through Oxide	Transmission Through Metals and Oxide
8.0	0.85	0.74
10.0	0.92	0.47
11.3	0.94	0.58
12.0	0.95	0.63

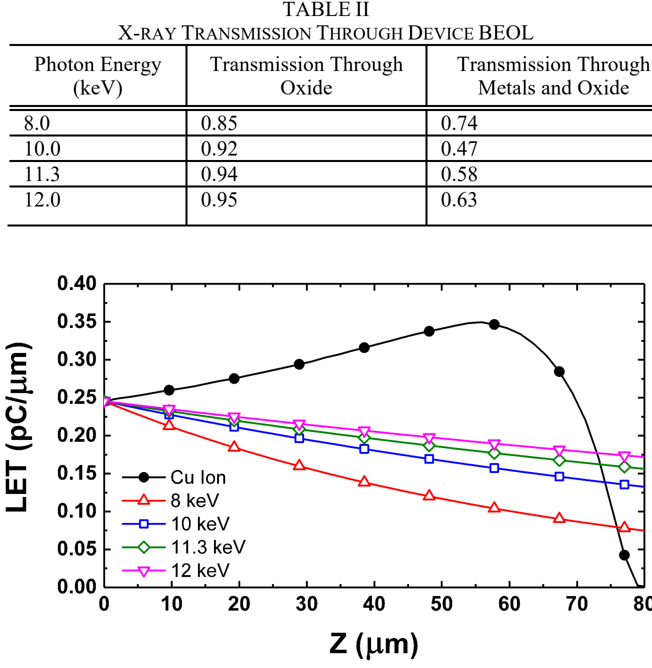

Fig. 2. Charge deposition profiles of Cu ion and X-ray pulses with equal surface LET. Ion LET is simulated using SRIM and X-ray LET is calculated using (1).

ion testing and can be obtained if the ion mass, energy, and incident material are known. The LET curve of a given ion can be simulated using SRIM [8]. Similarly, the X-ray LET curve can be calculated using the Gaussian beam equation given by (1). The surface LET used in this study is the LET of the ion or X-ray beam on the Si surface. For X-rays, that is

$$\mathrm{LET} = \mathrm{T} * \frac{\mathrm{E}}{3.6\ \mathrm{eV}}\alpha \tag{3}$$

where T is the transmission factor given by (2) and E is the pulse energy.

The LET curves for a Cu ion and X-ray beams with equal surface LET are shown in Fig. 2 for comparison. The 10-12 keV X-ray travels more than 90 μm and the 8 keV X-ray travels 45 μm in silicon before losing half of its energy. Having long penetration depth is an important factor for SiGe HBTs due to their long sensitive depth, well into the substrate [4].

IV. Experimental Results

A. Transient Peak Response

It has been previously shown in the literature that the SET response of SiGe HBTs involve two major mechanisms: 1) a fast drift current response due to charge deposition in the active device that creates a short-circuit path between the emitter and collector, via the so-called “ion-shunt effect,” and 2) a slower diffusion current “tail” resulting from the charge collection at the subcollector-substrate junction. The worst-case transient peak has been shown to occur for emitter-centered strikes (i.e., through the emitter/base/collector stack) [1]. The transient peak amplitude typically decreases as the beam moves away from the emitter [9]. However, the data obtained from pulsed X-ray, as

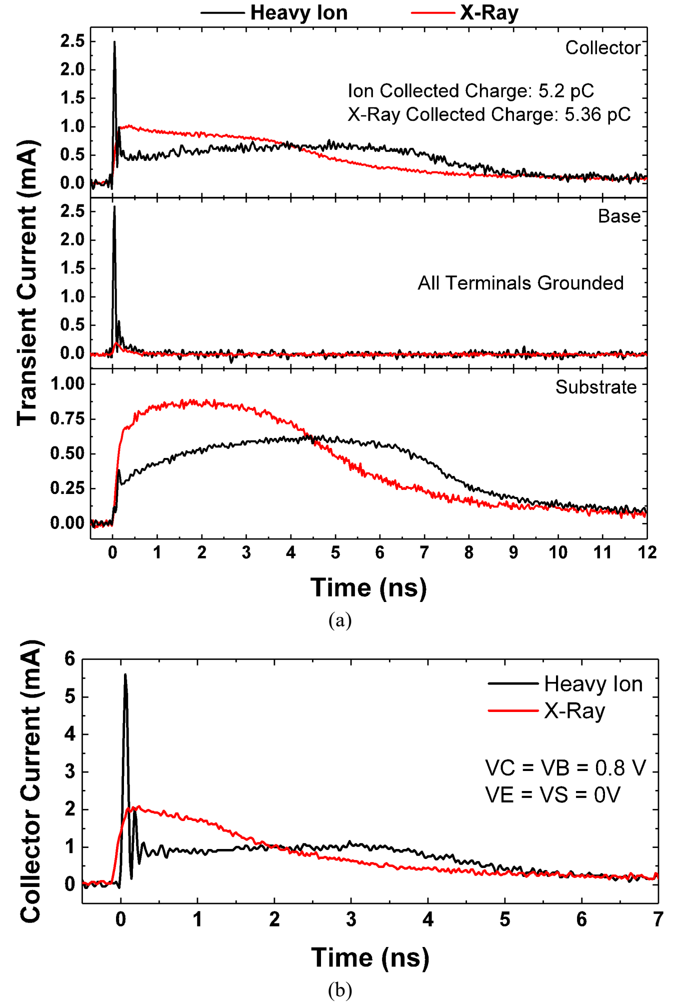

Fig. 3. Comparison of heavy-ion- and X-ray-induced SETs for a) the collector, base, and substrate terminal when all terminals are grounded and b) the collector terminal when the device is biased at VC = VB = 0.8 V, VE = VS = 0 V. A closer look of the collector current shows the slower transient rise from X-ray.

shown in Fig. 3, do not exhibit the traditional shunt effect observed in heavy-ion results. A closer look of the collector transient in Fig. 3b shows that the X-ray induced transient also has a slower rise time. Note that the device is biased in forward-active mode (turned on) in Fig. 3b because biasing the device in its on-state results in higher transient peaks. However, no fast drift current is observed with X-rays when the SiGe HBT is biased in forward-active mode.

There are two potential reasons for the lack of a fast transient peak: 1) The peak carrier densities deposited with pulsed X-ray are too low (higher carrier densities will exacerbate the shunt effect), and 2) the X-ray pulse width is too slow (the slow carrier generation will mask the fast drift current). The slow carrier generation can also result in slow transient rise time. To verify how these two factors affect SETs, TCAD simulations were performed. A 296 pJ beam with 10 keV photon energy, 102 ps pulse width and 1.61 μm spot size was chosen as a control because it has similar properties as the beam that produced the highest transient peak in the data. The charge density profile of the control beam is shown in Fig. 1. Beam

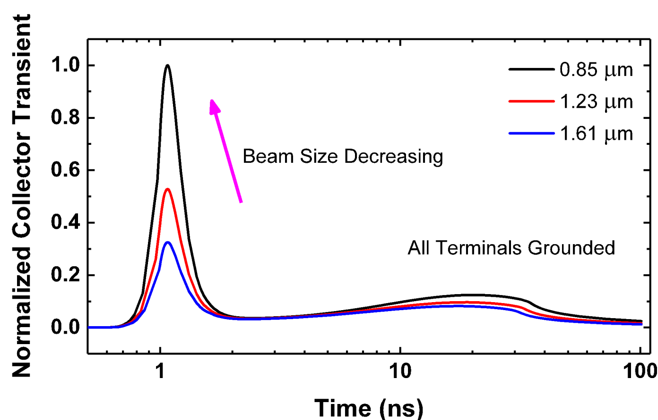

Fig. 4. Device SET induced by X-ray beams with spot sizes of 0.85 µm, 1.23 µm and 1.61 µm. Smaller beams deposit denser charge tracks that result in higher transient peak.

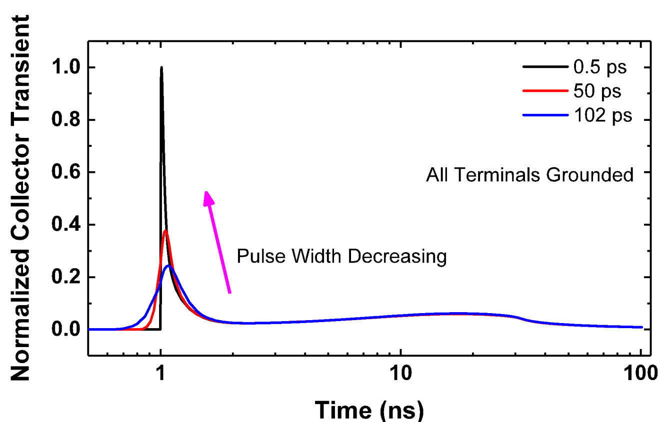

Fig. 5. Device SET induced by X-ray beams with pulse widths of 102 ps, 50 ps, and 0.5 ps. Faster beams result in higher transient peak.

spot size and pulse width were swept individually while everything else was held constant to isolate the effects from peak carrier density and pulse width, respectively.

Fig. 4 shows the changes in the transient peak across multiple beam spot sizes. The relationship between peak carrier density and the spot size of a Gaussian beam is inverse quadratic, as shown in (1). This means, for example, that if the spot size is reduced by a factor of two, the peak carrier density is increased by a factor of four. Although increasing pulse energy will increase the peak carrier density as well, it also will increase the collected charge. Therefore, pulse energy was not chosen as a variable to sweep. The result in Fig. 4 shows that the transient peak increases as spot size decreases. In addition, the transient tail gets larger with decreasing spot size, which means that charge collection is increasing. The detailed analysis of the effects of spot size on charge collection is discussed in the following section.

Fig. 5 shows the changes in the transient peak across multiple pulse widths. The simulation results show that pulse width also affects the transient peak but does not affect the collected charge. In addition, it verifies that the slower pulse width of X-ray causes slower transient rise. The 0.5 ps pulse width is chosen as the smallest value because it has been shown that pulse width of heavy ion charge generation, limited by impact

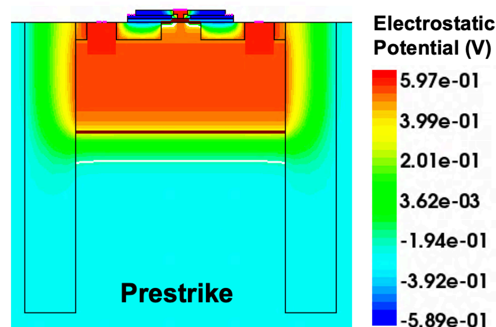

(a)

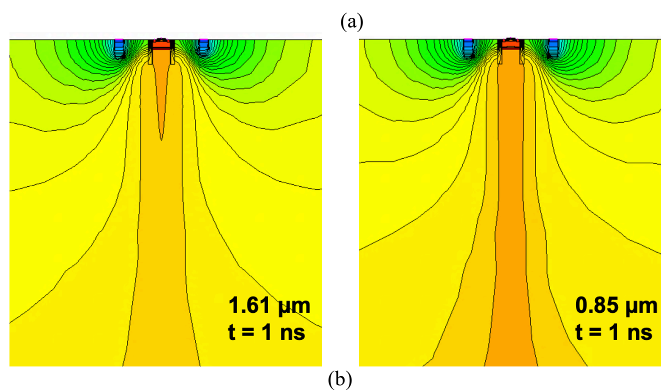

(b)

Fig. 6. Electrostatic potential of the device a) before X-ray strike and b) 1 ns after strike. Potential contour lines of SETs induced by similar beams with spot sizes of 1.61 µm and 0.85 µm are compared. The higher charge density of smaller beam pushes the CS junction deeper, increasing the charge collection depth by extending the sensitive depth.

ionization, is 0.5 ps [10]. Since the limitation is from the device itself, having a faster pulse will not further increase the peak. A similar transient comparison simulation with 0.5 ps and 0.1 ps pulses showed no difference in transients. Although both peak carrier density and pulse width affect transient peak, the peak carrier density appears to have more effect.

B. Charge Collection

The main charge collection mechanism for an ion strike inside the area of the SiGe HBT enclosed by deep trench (DT) of SiGe HBT is field-assisted diffusion current in the subcollector-substrate (CS) junction. Ion strikes inside the DT pushes the transient CS junction deeper into the substrate. The junction field causes enhanced charge collection from deeper in the device, often exceeding 10 µm [4].

In Fig. 4, the smaller spot size not only produced a higher transient peak but also a higher collected charge. For the largest spot size in Fig. 4, 97% of the beam is inside the DT, which means that the charge deposition in the sensitive area is equal for all three simulated spot sizes. Since the CS junction field is mainly responsible for deep charge collection, the electrostatic equipotential lines have been compared for the transients induced by the largest and smallest beams and are shown in Fig. 6. Even though the two beams have the same LET, the beam with the smaller spot size generates higher charge density, which in turn pushes the CS junction deeper into the substrate. As the junction extends, the sensitive depth of the device also increases.

For a given X-ray pulse energy, the collected charge should

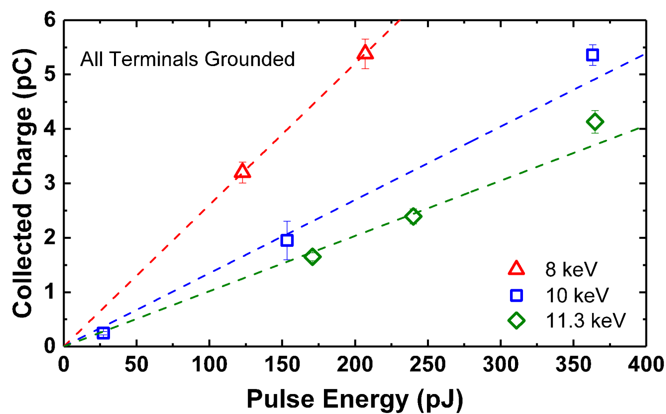

(a)

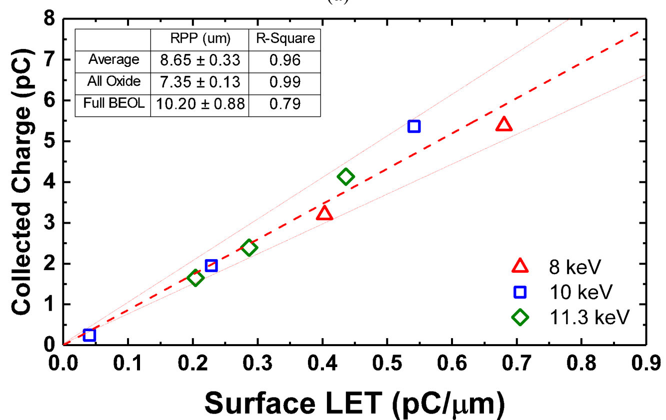

(b)

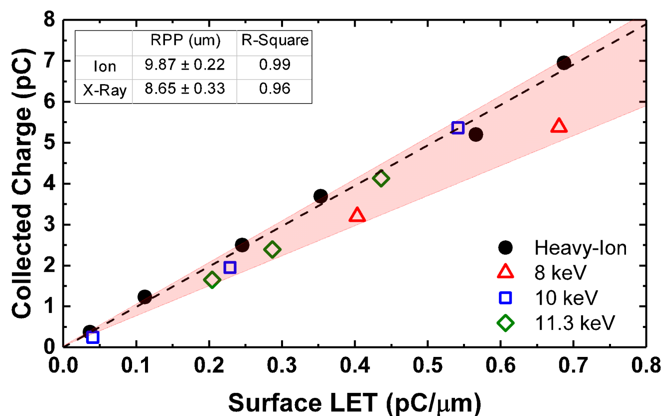

(c)

Fig. 7. CC data for SET induced by X-ray with multiple photon energies a) plotted against pulse energy and b) surface LET. The CC has a linear correlation with LET regardless of photon energy. c) The CC dependence on LET of X-ray is compared with that of heavy ion. For a given surface LET, more charge is collected from ion because the ion deposits more charge in the sensitive depth.

decrease as penetration depth increases due to changing photon energies, as shown in Fig. 7a. If the pulse energy is fixed (meaning the deposited charge across the entire charge track is fixed), the pulse with the larger penetration depth will deposit more of its charge deeper in the substrate, where charge collection efficiency is decreased [11]. However, collected charge with respect to surface LET, as plotted in Fig. 7b, is linear, with no photon energy dependence. The surface LET was calculated for both best and worst case BEOL options, as

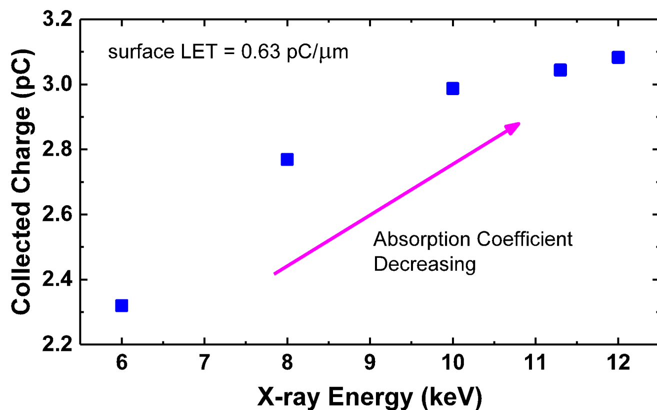

Fig. 8. The simulated charge collection of X-ray beams with surface LET of 0.63 pC/µm. For a given surface LET, pulses with higher X-ray energy deposits more charge in the sensitive volume. Higher charge deposition in the sensitive volume results in higher charge collection.

discussed in Section II, to give a confidence interval. The average of the two is a good approximation when the beam strikes on the center of the device. The slope of the curves, also known as Rectangular Parallelepiped (RPP) thickness, were calculated to compare charge collection efficiency for the different beams. For a given LET, a device with higher RPP results in higher collected charge [4]. Fig 7c shows a comparison between heavy ion and X-ray collected charge measurements. Note that, results from both irradiation sources show a strong linear correlation between surface LET and collected charge. Since the charge collection from both ion and X-ray are linear, X-ray equivalent LET can be calculated from the correlation. For 8-12 keV pulses, the correlation factor for X-ray equivalent LET is 1.14, which is obtained by comparing the X-ray RPP with that of the heavy ion.

The RPP extracted using heavy-ion data is larger than that extracted using X-ray data. There are two reasons for this discrepancy:

1) an ion beam has smaller spot size so as discussed earlier in this section, the charge collection from an ion strike will be higher for same LET.
2) The RPP approach assumes constant LET throughout the sensitive depth of the device. This approximation works for devices with short sensitive depth but is not accurate for SiGe HBTs due to their deep sensitive volume. For example, if charge deposition from a Cu ion and 10 keV X-ray with equal surface LET were compared for a device with an RPP thickness of 15 µm, the deposited charge in that thickness will be 3.9 pC and 3.5 pC for the ion and X-ray pulse, respectively. A larger amount of deposited charge will result in more charge collection.

The second reason leading to a larger RPP thickness for heavy-ion data compared to X-ray pulses also implies that that an X-ray pulse with absorption coefficient much higher or lower than those of 8-12 keV pulses will not have the same linear correlation with CC. To confirm this observation, charge collection from pulses with equal surface LET but different absorption coefficients are compared in Fig. 8. The absorption coefficient of 6 keV X-rays in silicon is 334 cm^{-1}, which is 7.5

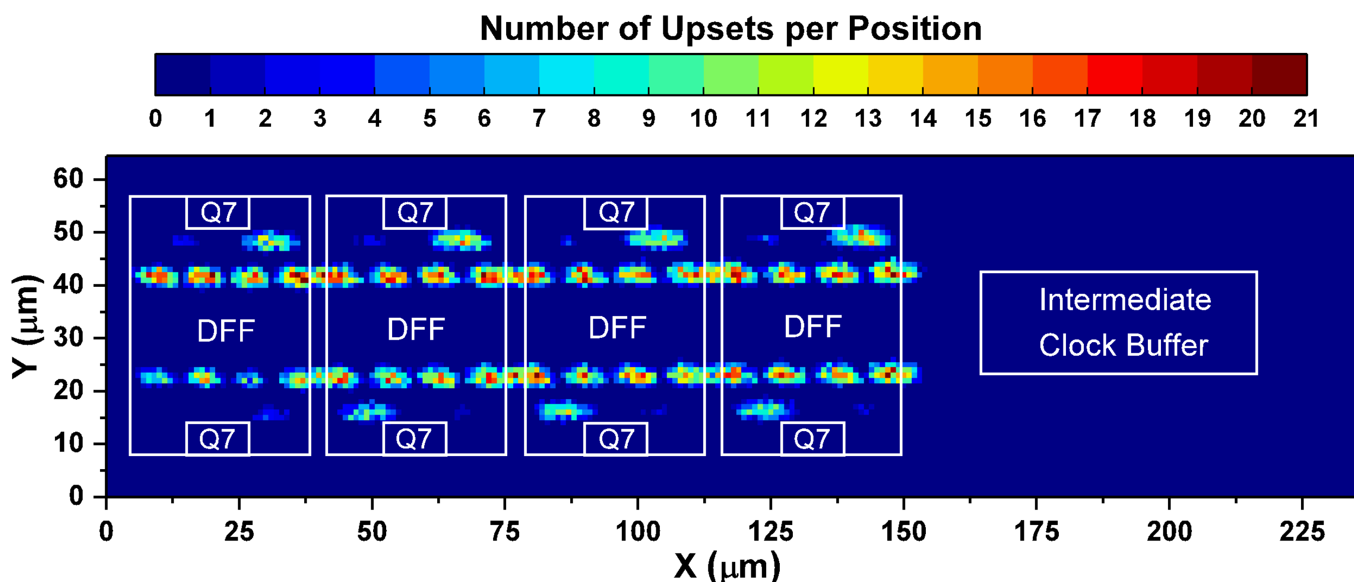

Fig. 9. SEU raster scan of a 16-bit MS shift-register. The scan was taken on four of the sixteen D-flip flops and one of the four clock buffers. No upsets were measured when the beam was scanned across the clock buffer because it was hardened using the gated-feedback cell technique.

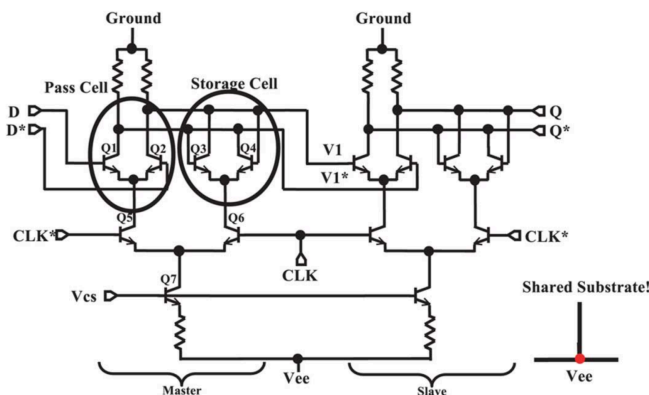

Fig. 10. Schematic of standard current-mode-logic MS DFF [13].

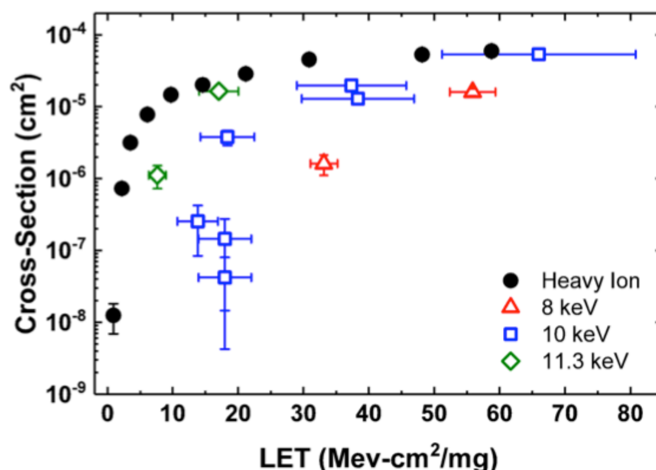

Fig. 11. The error cross-section vs. LET of heavy ion and X-ray induced SEU in standard MS SR.

times higher than that of 12 keV X-rays. The absorption coefficients of the rest of the pulses are given in Table I. The simulation results show that charge collection increases as the photon energy increases. As photon energy increases, absorption coefficient decreases, which means the LET of the beam decays less across depth. Therefore, for a fixed surface LET, the beam with higher photon energy will deposit more charge in the sensitive area.

C. Shift-Register SEU

The device-level X-ray data showed that it cannot produce the fast drift current present in transients induced by ion, making it less desirable for testing applications where transient peak is important to the SEE response of a circuit. However, it should still be a very good source for SEE studies where charge collection is the dominant mechanism.

SiGe digital logic circuits are extremely sensitive to SEU. In high-speed logic circuits, the charge generated from ionizing particles corrupt data over several clock cycles. The circuit response to single events depend on the circuit design, operating current and incident beam LET [12]. Pulsed X-rays can give valuable information about circuit sensitive nodes. To verify this assertion, a 16-bit standard MS shift register with unhardened D-flip flops (DFF) and hardened clock trees was tested using both X-rays and heavy ions. The circuit is designed using NPN transistors with an emitter area of 0.12x1.00 μm^2. The area inside the DT is 1.98 x 2.72 μm^2. The circuit design is identical to the standard MS SR in [13]. The X-ray beam was scanned across the four of the 16 DFFs in the SR. The number of upsets at each position was recorded after exposing the part to 154050 X-ray pulses. These upsets are plotted as a function of X-ray strike location in Fig. 9. The schematic of the DFF is given in Fig. 10. The raster scan shows the sensitive nodes in the DFFs clearly. The clock buffer did not get upset, as it was already radiation hardened [13].

The error cross-section curve was obtained from X-ray induced bit errors and compared to that of heavy ion and is shown in Fig. 11. The error cross-section of the X-ray is calculated as [14]

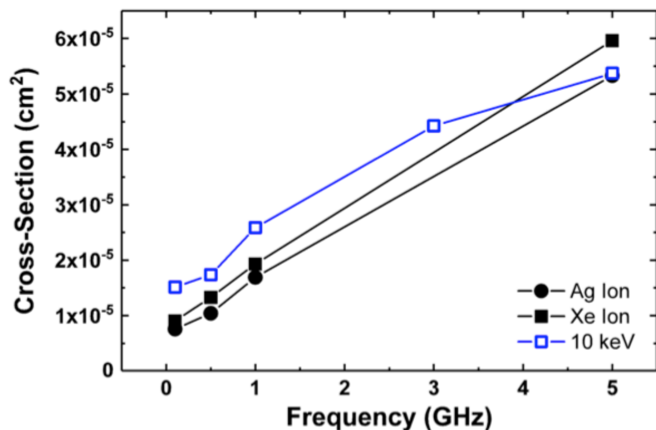

Fig. 12. The error cross-section vs. clock frequency of SEU induced by ion and X-ray.

$$\sigma(\mathrm{cm}^2) = \frac{\text{Number of Events}}{\text{Number of Pulses}} * Scan\ Area(cm^2) \qquad (3)$$

The confidence interval of the X-ray surface LET, calculated for best-case scenario, (i.e., all oxide layers in the BEOL), and worst-case scenario, (i.e., with metal layers present in the BEOL), is plotted as error bars on the x-axis. No correction factor was made to adjust the LET for the beam spot size or differences in ion and X-ray RPPs. The non-adjusted X-ray cross-section curve clearly does not match with heavy-ion data. In addition, the cross-section vs. LET of X-ray pulses with different photon energies do not fall on the same curve. However, how much the X-ray cross-section data point is shifted in the x-axis appears to increase as the X-ray photon energy decreases. The RPP of X-ray decreases with increasing absorption coefficient, which increases as the photon energy decreases [6]. The device-level charge collection study showed that the RPP of X-rays is smaller than that of heavy ions, and the difference grows as the X-ray energy decreases. For X-rays, the actual effective LET is lower than the surface LET. For most heavy ions used for SEE testing, the actual effective LET is higher than the surface LET because ion LET increases with depth (which is the case for the ions used in this study. An ion LET decreases with depth after its Bragg peak [15].)

For X-ray energies of 8-12 keV, the RPP did not change much when all the terminals of the device were grounded. This may not hold true in digital circuits, since the substrate is typically biased around -5V to isolate the substrate noise. The substrate of the SR in this study was biased at -5.2 V. When the substrate-subcollector junction is reverse biased, charge collection increases as the junction field is stronger, therefore pulls more charge. A stronger CS junction field will extend the sensitive depth. The extended sensitive depth will amplify the differences in RPP between ion and X-ray. If the differences in the RPP of X-ray and ion induced transients were taken into account, all the X-ray cross-section curves in Fig. 11 would be shifted to the left, with the 8 keV curve shifted the most. More in-depth analysis is needed to quantify these effects for proper calculation of effective X-ray LET and possible effects from the X-ray spot size. However, this is beyond the scope of this paper and will be the topic of a future study.

In Fig. 11, the cross-section of the highest LET when using a 10 keV pulse is similar to that of Xe ion and Ag ion, which are the two highest ion LET points in the ion data. The same beam conditions were used to verify the dependence of SEU cross-section as a function of SR data rate. Fig. 12 shows that the X-ray data match heavy-ion data very well across all measured clock frequencies. These results suggest that X-ray pulses could be used for accurate relative measurements, i.e., capture differences in error cross-section due to changes in bias voltages, data rate, and circuit topology. Additional work is required before quantitative agreement between X-ray and ion data can be achieved, at least for designs using SiGe HBTs.

V. Discussion

Although X-rays are able to penetrate metals, their absorption in metals significantly reduces their energy. Generally, X-ray transmission increases exponentially with photon energy until it reaches its absorption edge. At the absorption edge, a sharp discontinuity occurs, and the absorption increases. It continues decreasing again as the energy increases. For copper, the absorption edge is at 8.98 keV, which is why the 10 keV beam has a lower transmission factor than the 8.0, 11.3 and 12.0 keV beams. Tungsten has two absorption edges, at 10.2 keV and 11.5-12.1 keV. Since the X-ray absorption coefficients of materials are well-defined, the X-ray energies with the highest transmission factors can be chosen if the type of metals in the DUT BEOL are known. If the BEOL of the device is not known, a high photon energy, such as 20 keV, can be chosen to minimize the energy loss across different types of materials. Choosing a high photon energy can also be advantageous because the LET of a beam with smaller absorption coefficient decays more slowly as a function of depth. However, for a fixed LET, the pulse with lower absorption coefficient requires more pulse energy. The highest available flux varies with photon energy at APS. Therefore, there is a tradeoff between energy loss in metal, LET decay, and highest surface LET. The optimal combination of these three factors depends on the DUT.

VI. Summary

This paper has presented the first single-event effects investigation using pulsed X-rays in SiGe HBTs. The results from pulsed x-ray experiments were compared to heavy ion data. The transient peak current in the emitter-base and base-collector junction, induced by ion-shunt effect, was not present in X-ray transients. TCAD simulations showed that the lack of peak current was caused by the fact that the peak carrier density induced by X-rays was too low and the pulse width was too slow to shunt the heavily-doped base of the SiGe HBT. The charge collected from X-rays show good correlation with that of ion beam at the device level. The BEOL of the device reduced the beam energy significantly, especially at certain photon energies depending on the type of metal present in the device. Circuit-level SEU results using standard MS shift registers showed that X-rays are useful for identifying the sensitive nodes in a circuit. A more detailed study is needed to enable circuit-level ion to X-ray correlation.

References

[1] J. D. Cressler, “Radiation effects in SiGe technology,” IEEE Trans. Nucl. Sci., vol. 60, no. 3, pp. 1992–2014, Jun. 2013.

[2] S. P. Buchner, F. Miller, V. Pouget, and D. P. McMorrow, "Pulsed-laser testing for single-event effects investigations", IEEE Trans. Nucl. Sci., vol. 60, no. 3, pp. 1852-1875, Jun. 2013.

[3] D. M. Cardoza, S. D. LaLumondiere, M. A. Tockstein, S. C. Witczak, Y. Sin, B. J. Foran, W. T. Lotshaw, and S. C. Moss, "Single Event Transients Induced by Pulsed X-Ray Absorption in III-V Heterojunction Transistors", IEEE Trans. Nucl. Sci., vol. 59, no. 6, pp. 2729–2737, Dec. 2012.

[4] Enrique J. Montes, Robert A. Reed, Jonathan A. Pellish, Michael L. Alles, Ronald D. Schrimpf, Robert A. Weller, Muthubalan Varadharajaperumal, Guofu Niu, Akil K. Sutton, Ryan Diestelhorst, Gustavo Espinel, Ramkumar Krithivasan, Jonathan P. Comeau, John D. Cressler, Paul W. Marshall, and Gyorgy Vizkelethy, "Single Event Upset Mechanisms for Low-Energy-Deposition Events in SiGe HBTs", IEEE Trans. Nucl. Sci., vol. 55, no. 3, pp. 1581–1586, Jun. 2008.

[5] D. Cardoza, Stephen D. LaLumondiere, N. P. Wells, M. A. Tockstein, D. L. Brewe, W. T. Lotshaw, S. C. Moss, "Investigating Pulsed X-Ray Induced SEE in Analog Microelectronic Devices", IEEE TNS, vol. 62, no. 6, pp. 2458-2467, Dec. 2015.

[6] J. H. Hubbell, S. M. Seltzer, "X-ray Mass Attenuation Coefficients", National Institute of Standards and Technology, Accessed: Nov. 20. 2018, [Online]. Available: http://physics.nist.gov/PhysRefData/XrayMassCoef/cover.html

[7] J. M. Hales, A. Khachatrian, S. Buchner, N. J.-H. Roche, J. Warner, and D. McMorrow, "A simplified approach for predicting pulsed-laser-induced carrier generation in semiconductor," IEEE Trans. Nucl. Sci., vol. 64, no. 3, pp. 1006–1013, Mar. 2017.

[8] J. F. Ziegler, J. P. Biersack, and M. D. Ziegler. SRIM. Accessed: Jan. 20, 2019. [Online]. Available: http://www.srim.org/SRIM/SRIM2011.htm

[9] Z. E. Fleetwood, N. E. Lourenco, A. Ildefonso, J. H. Warner, M. T. Wachter, J. M. Hales, G. N. Tzintzarov, N. J. Roche, A. Khachatrian, S. P. Buchner, D. McMorrow, P. Paki, and J. D. Cressler, "Using TCAD Modeling to Compare Heavy-Ion and Laser-Induced Single Event Transients in SiGe HBTs," IEEE Trans. Nucl. Sci., vol. 64, no. 1, pp. 398–405, Jan. 2017.

[10] P. Oldiges, R. Dennard, D. Heidel, B. Klaasen, F. Assaderaghi, M. Jeong, "Theoretical determination of the temporal and spatial structure of /spl alpha/-particle induced electron-hole pair generation in silicon," IEEE Trans. Nucl. Sci., vol. 47, no. 6, pp 2575-2579, Dec. 2000.

[11] J. A. Pellish et al., "A generalized SiGe HBT single-event effects model for on-orbit event rate calculations," IEEE Trans. Nucl. Sci., vol. 54, no. 6, pp. 2322–2329, Dec. 2007.

[12] P. W. Marshall, M. A. Carts, A. Campbell, D. McMorrow, S. Buchner, R. Stewart, B. Randll, B. Gilbert, and R. Reed, "Single event effects in circuit hardened SiGe HBT logic at gigabit per second data rate," IEEE Trans. Nucl. Sci., vol. 47, pp. 2669–2674, Dec. 2000.

[13] R. Krithivasan, P.W. Marshall, M. Nayeem, A.K. Sutton, W. Kuo, , B.M. Haugerud,L. Najafizadeh, J. D. Cressler, M.A. Carts, C J. Marshall, D L. Hansen, K. M. Jobe, A.L. McKay, G. Niu, R. Reed, B. A. Randall, C. A. Burfield, M.Daun-Lindberg, B. Gilbert, E. Daniel, "Application of RHBD Techniques to SEU Hardening of Third- Generation SiGe HBT Logic Circuits," IEEE Trans. Nucl. Sci, vol. 53, no. 6, p. 3400-3407, Dec. 2006.

[14] F. Miller, N. Buard, T. Carriere, R. Dufayel, R. Gaillard, P. Poirot *et al.*, "Effects of beam spot size on the correlation between laser and heavy ion SEU testing," *IEEE Trans. Nucl. Sci.*, vol. 51, no. 6, pp. 3708–3715, Dec. 2004.

[15] A. Ildefonso, Z. E. Fleetwood, G. N. Tzintzarov, J. M. Hales, D. Nergui, M.Frounchi, A. Khachatrian, S. P. Buchner , D. McMorrow, J. H. Warner, J. Harms, A. Erickson, K. Voss , V. Ferlet-Cavrois, and J. D. Cressler, "Optimizing optical parameters to facilitate correlation of laser- and heavy-ion-induced single-event transients in SiGe HBTs", *IEEE Trans. Nucl. Sci.*, vol. 66, no. 1, pp. 359–367, Jan. 2019.